Supporting information

Thickness Dependent Magnetic Transition in Few Layer 1T Phase $CrTe_2$

Pengfei Gao,† Xingxing Li,*,†,‡ and Jinlong Yang*,†,‡

†Synergetic Innovation Center of Quantum Information and Quantum Physics, University of Science and Technology of China, Hefei, Anhui 230026, China

‡Hefei National Laboratory for Physical Sciences at the Microscale, University of Science and Technology of China, Hefei, Anhui 230026, China

Email: lixx@ustc.edu.cn; jlyang@ustc.edu.cn

COMPUTATIONAL DETAILS

Density functional theory calculations are performed using the generalized gradient approximation for the exchange-correlation potential, the projector augmented wave method, and a plane-wave basis set as implemented in the Vienna ab-initio simulation (VASP).[1] An energy cutoff of 400 eV for plane waves is adopted. For bulk $CrTe_2$, a 14 × 4 × 4 k-point mesh is used to sample the first Brillouin Zone of the adopted $1 \times 2\sqrt{3} \times 2$ rectangular supercell. For few layer $CrTe_2$, a 7 × 4 × 1 k-point mesh is used to sample the first Brillouin Zone of the adopted $2 \times 2\sqrt{3} \times 1$ rectangular supercell. For charge density wave (CDW) phase of monolayer $CrTe_2$, a 9×9×1 k-point mesh is used to sample the first Brillouin Zone of the adopted $\sqrt{3} \times \sqrt{3} \times 1$ hexagonal supercell. The Monkhorst-Pack method of k point sampling is used.[2] For few layer $CrTe_2$, a vacuum region of 15 Å is added along the c lattice direction so that the interactions between the slab and its periodic image can be neglected. All atoms are allowed to relax until the residual force per atom is less than 0.01 eV/ Å. The energy convergence criterion is set as 1E-6 eV. The vdw correction has been tested in detail (listed in Table S1). The lattice constant calculated by the opt-B86-vdW functional[3-6] (a=3.789 Å, c=6.079 Å) is in good agreement with the experimental value (a=3.789 Å, c=6.096 Å). Therefore, we choose opt-B86-vdW functional for all structural optimization.

The influence of effective U values of Cr_3d is tested in detail. The calculated lattices, magnetic moments, magnetic anisotropy energies, Curie temperatures and interlayer exchange energies for bulk $CrTe_2$ with different effective U values are listed in Table S2. The available experimental values are also given. Results show that the calculated Curie temperature decreases as the U value increases, which are comparable to the experimental value (310 K) as long as U < 1.5 eV, while an effective U value greater than 1.5 eV predicts the ground interlayer magnetic coupling of bulk $CrTe_2$ to be falsely AFM. Moreover, +U method give too large lattice and magnetic moment compared with the experimental values. Considering these points, the results presented in the main text are calculated without +U correction. Since the hybrid functional is usually more accurate than the +U correction, we test HSE06 functional and find that the ground interlayer magnetic coupling of bulk $CrTe_2$ is also falsely predicted to be AFM, i.e. the energy of interlayer AFM state is 17 meV/Cr lower than that of interlayer FM state. Besides, the magnetic

moment per formula calculated by the HSE06 functional is 2.58 μB/f.u., which is much larger than the experimental value (1.7 μB/f.u.). Therefore, HSE06 functional is not considered in the calculations of few layer $CrTe_2$.

In order to calculate the exchange parameters of the bulk $CrTe_2$, we consider the following six magnetic structures shown in Figure S1. Magnetic energies of these magnetic configurations in each magnetic unit cell read as follow:

$$E_a = E_0 + \frac{N^2}{4} \times \frac{1}{2} (6J_1 + 6J_2 + 2J_3 + 12J_4)$$

$$E_b = E_0 + \frac{N^2}{4} \times \frac{1}{2} (-2J_1 - 2J_2 + 2J_3 - 4J_4)$$

$$E_c = E_0 + \frac{N^2}{4} \times \frac{1}{2} (2J_1 - 2J_2 + 2J_3 + 4J_4)$$

$$E_d = E_0 + \frac{N^2}{4} \times \frac{1}{2} (6J_1 + 6J_2 - 2J_3 - 12J_4)$$

$$E_e = E_0 + \frac{N^2}{4} \times \frac{1}{2} (-2J_1 - 2J_2 - 2J_3 + 4J_4)$$

$$E_f = E_0 + \frac{N^2}{4} \times \frac{1}{2} (2J_1 - 2J_2 - 2J_3 - 4J_4).$$

Here, N represents the number of unpaired electrons on each Cr atom, which is chosen as 2 in our calculations. Then, we solve the exchange parameters of bulk $CrTe_2$ (listed in Table S4) using the least square method.

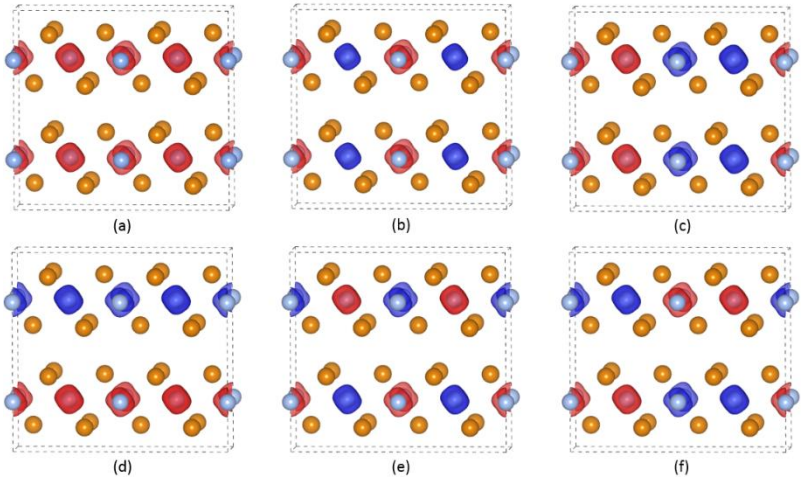

Figure S1. (a-f) Spin densities of six magnetic orders used for solving exchange parameters of bulk $CrTe_2$ with an isosurface value of 0.04 e/Bohr^3. Red and blue contours represent spin-up and -down, respectively. The blue-gray and dark yellow balls represent Cr and Te atoms, respectively.

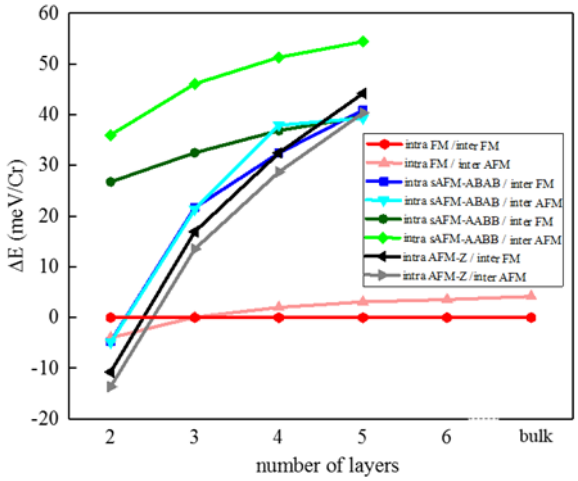

Figure S2. The total energies at eight different magnetic states by setting the energy of FM state to be zero calculated with effective U value of Cr_3d being 1.2 eV. The FM, sAFM-ABAB, sAFM-AABB and AFM-Z before the slash indicate intralayer coupling, and the FM and AFM after the slash indicate interlayer coupling. The critical number of layers for intra and interlayer AFM-FM transition is reduced from 5 (U=0 eV) to 3 (U=1.2 eV).

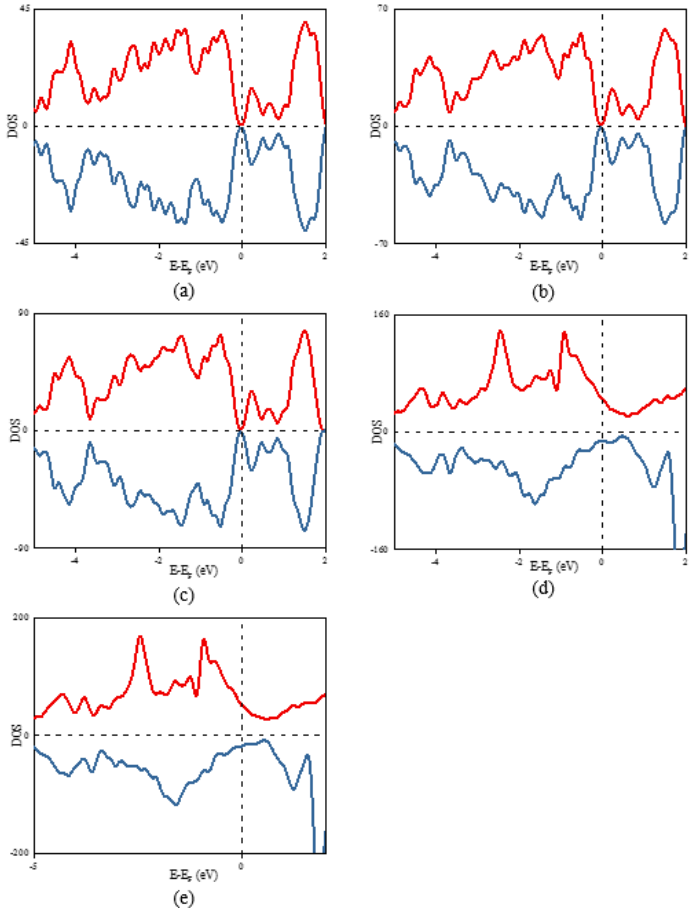

Figure S3. (a-e) Density of states (DOS) for the most stable 2-, 3-, 4-, 5- and 6-layer $CrTe_2$ nanosheets, respectively. The red (blue) line represents the DOS of the up (down) spin channel. Fermi levels are all set to zero.

Table S1. Optimized lattice constants of bulk $CrTe_2$ with different vdW corrections.

	No correction	dDsC[7]	D2-Grimme[8]	D3-Grimme[9]	D3-BJ[10]	T-S[11]	Many-body[12]
a (Å)	3.827	3.778	3.778	3.787	3.750	3.837	3.731
c (Å)	6.203	6.032	6.215	5.965	5.917	5.862	6.062
	optB86b[6]	optB88[6]	optPBE[6]	DF2[13]	rDF2[14]	Exp[15]	
a (Å)	3.789	3.828	3.852	3.983	3.793	3.789	
c (Å)	6.079	6.160	6.232	6.465	6.075	6.096	

Table S2. The calculated lattice constants, magnetic moment per formula (M), magnetic anisotropy energies (MAE), Curie temperatures (T_c) and interlayer exchange energies (E_{ex}=E (FM)-E (AFM)) of bulk $CrTe_2$ with different effective U values.

U_{eff} (eV)	0.0	0.5	1.0	1.5	2.0	Exp[15]
Lattice (Å)	3.789	3.804	3.819	3.836	3.858	3.789
M (μB/f.u.)	2.43	2.49	2.56	2.61	2.693	1.7
MAE (meV/f.u.)	0.7	1.2	0.4	1.1	1.5	>0
T_c (K)	359	356	333	-	-	310
E_{ex} (meV/Cr)	-17.5	-12.0	-6.5	-1.0	3.0	<0

Table S3. Structural information of 1T-$CrTe_2$ nanosheets with different thicknesses at different intralayer magnetic states: (a) intra FM, (b) intra sAFM-ABAB, (c) intra s-AABB and (d) intra AFM-Z. The interlayer magnetic coupling is set as FM.

(a)

	lattice constant of a' (Å)	lattice constant of b' (Å)	interlayer Cr-Cr distance (Å)
monolayer	7.320	12.656	-
2-layer	7.501	12.996	6.093
3-layer	7.506	13.000	6.113
4-layer	7.527	13.034	6.111
5-layer	7.550	13.038	6.103

(b)

	lattice constant of a' (Å)	lattice constant of b' (Å)	interlayer Cr-Cr distance (Å)
monolayer	7.401	11.969	-
2-layer	7.422	12.057	6.830
3-layer	7.508	12.356	6.418
4-layer	7.510	12.362	6.447
5-layer	7.530	12.366	6.452

(c)

	lattice constant of a' (Å)	lattice constant of b' (Å)	interlayer Cr-Cr distance (Å)
monolayer	7.362	12.024	-
2-layer	7.378	12.670	6.227
3-layer	7.424	12.738	6.205
4-layer	7.442	12.815	6.182
5-layer	7.450	12.799	6.202

(d)

	lattice constant of a' (Å)	lattice constant of b' (Å)	interlayer Cr-Cr distance (Å)
monolayer	7.141	12.301	-
2-layer	7.163	12.350	6.930
3-layer	7.167	13.374	6.932
4-layer	7.168	13.380	6.936
5-layer	7.167	13.380	6.959

Table S4. Exchange parameters of bulk $CrTe_2$ with different effective U values.

U_{eff} (eV)	0.0	0.5	1.0
J_1 (meV)	-6.5625	-8.0938	-9.2813
J_2 (meV)	-9.1875	-8.5781	-7.8906
J_3 (meV)	-5.6671	-5.2031	-4.8385
J_4 (meV)	-0.8281	-0.5547	-0.3516

Reference

(1) Kresse, G. Furthmüller, J. Efficient Iterative Schemes for ab Initio Total-energy Calculations Using a Plane-wave Basis Set. *Phys. Rev. B* **1996**, *54*, 11169-11186.

(2) Monkhorst, H. J.; Pack, J. D. Special Points for Brillouin-zone Integrations. *Phys. Rev. B* **1976**, *13*, 5188-5192.

(3) Dion, M.; Rydberg, H.; Schroder, E.; Langreth, D. C.; Lundqvist, B. I. Van Der Waals Density Functional for General Geometries. *Phys. Rev. Lett.* **2004**, *92*, 246401.

(4) Roman-Perez, G.; Soler, J. M. Efficient Implementation of a Van Der Waals Density Functional: Application to Double-Wall Carbon Nanotubes. *Phys. Rev. Lett.* **2009**, *103*, 096102.

(5) Klimeš, J.; Bowler, D. R.; Michaelides, A. Van der Waals Density Functionals Applied to Solids. *Phys. Rev. B* **2011**, *83*, 195131.

(6) Klimes, J.; Bowler, D. R.; Michaelides, A. Chemical Accuracy for The Van Der Waals Density Functional. *J. Phys. Condens. Matter* **2010**, *22*, 022201.

(7) Steinmann, S. N.; Corminboeuf, C. Comprehensive Benchmarking of a Density-Dependent Dispersion Correction. *J. Chem. Theory Comput.* **2011**, *7*, 3567-3577.

(8) Grimme, S. Semiempirical GGA-type Density Functional Constructed with A Long-Range Dispersion Correction. *J. Comput. Chem.* **2006**, *27*, 1787-1799.

(9) Grimme, S.; Antony, J.; Ehrlich, S.; Krieg, H. A Consistent and Accurate Ab Initio Parametrization of Density Functional Dispersion Correction (DFT-D) For the 94 Elements H-Pu. *J. Chem. Phys.* **2010**, *132*, 154104.

(10) Grimme, S.; Ehrlich, S.; Goerigk, L. Effect of The Damping Function in Dispersion Corrected Density Functional Theory. *J. Comput. Chem.* **2011**, *32*, 1456-1465.

(11) Tkatchenko, A.; Scheffler, M. Accurate Molecular Van Der Waals Interactions from Ground-State Electron Density and Free-Atom Reference Data. *Phys. Rev. Lett.* **2009**, *102*, 073005.

(12) Tkatchenko, A.; DiStasio, R. A., Jr.; Car, R.; Scheffler, M. Accurate and Efficient Method for Many-Body Van Der Waals Interactions. *Phys. Rev. Lett.* **2012**, *108*, 236402.

(13) Lee, K.; Murray, É. D.; Kong, L.; Lundqvist, B. I.; Langreth, D. C. Higher-Accuracy Van Der Waals Density Functional. *Phys. Rev. B* **2010**, *82*, 081101.

(14) Hamada, I. Van Der Waals Density Functional Made Accurate. *Phys. Rev. B* **2014**, *89*, 121103.

(15) Freitas, D. C.; Weht, R.; Sulpice, A.; Remenyi, G.; Strobel, P.; Gay, F.; Marcus, J.; Nunez-Regueiro, M. Ferromagnetism in Layered Metastable 1T-$CrTe_2$. *J. Phys. Condens. Matter* **2015,** *27*, 176002.